Stem Cell Reports, Volume *10*

Supplemental Information

Exosome-Mediated Benefits of Cell Therapy in Mouse and Human Models of Duchenne Muscular Dystrophy

Mark A. Aminzadeh, Russell G. Rogers, Mario Fournier, Rachel E. Tobin, Xuan Guan, Martin K. Childers, Allen M. Andres, David J. Taylor, Ahmed Ibrahim, Xiangming Ding, Angelo Torrente, Joshua M. Goldhaber, Michael Lewis, Roberta A. Gottlieb, Ronald A. Victor, and Eduardo Marbán

Figure S1. *Related to Figure 1; Changes in ventricular volumes and engraftment with alterations in transcriptomic and proteomic profiles underlying CDC injection in the mdx heart.*

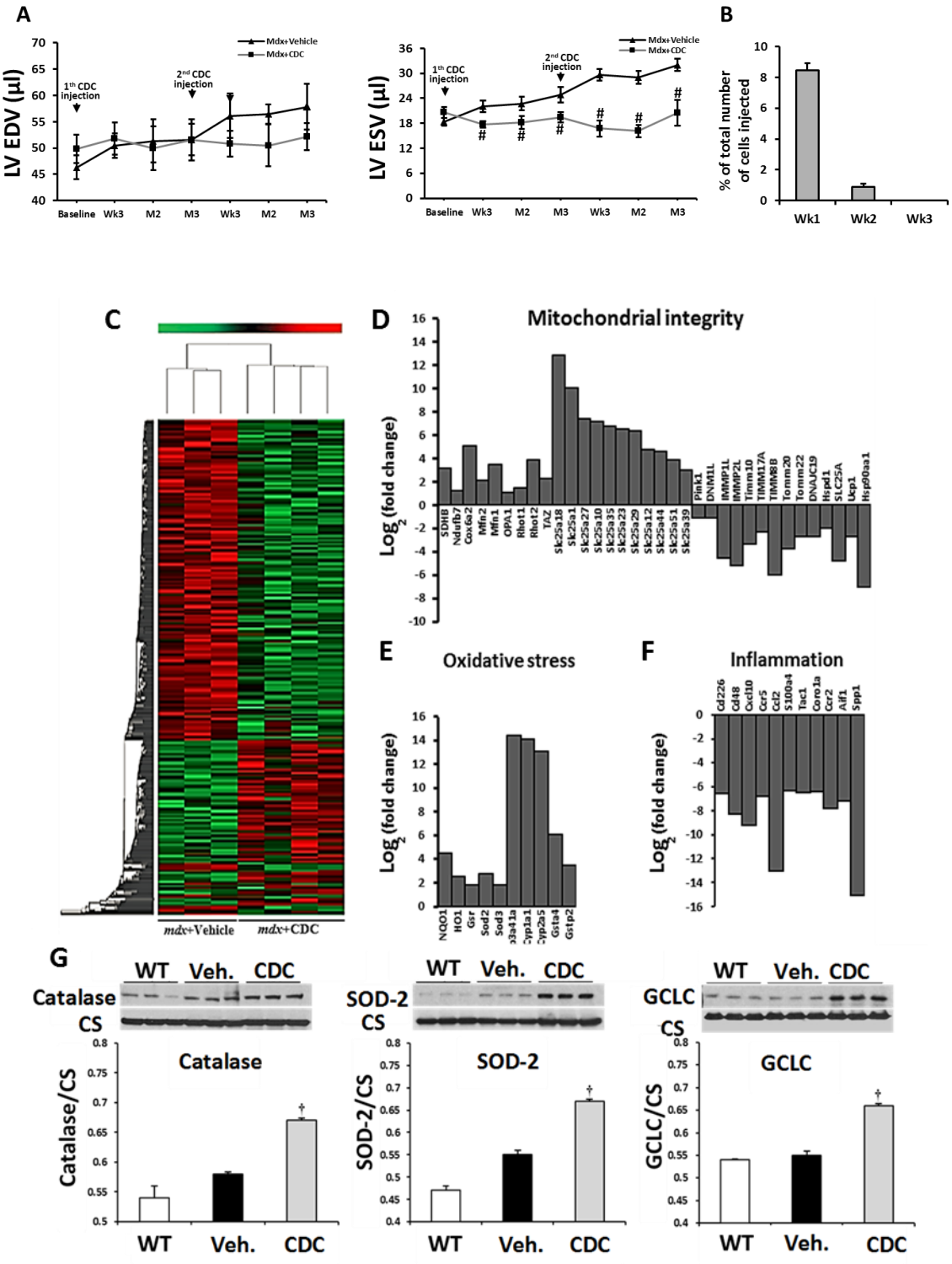

A: Left ventricular end-diastolic (LV EDV) and end-systolic (LV ESV) volumes after cardiosphere-derived cell (CDC) administration. CDC transplantations resulted in a sustained improvement of LV ESV for 3 months after both first and second (3 months interval) injections in *mdx* mice (Mdx+CDC), relative to placebo (Mdx+Vehicle). Differences in LV EDV were more marked after the second injection but were not significant. B: Percentage engraftment of CDCs in the heart 1, 2 and 3 weeks after transplantation. Percentage engraftment of CDCs at 1 week was ~8% and <1% at 2 weeks. By 3 weeks, no surviving CDCs could be detected. n = 3 at each time point. C: Changes in *mdx* heart transcriptome 3 wks after CDC treatment. 2-Dimensional hierarchical clustering using 560 genes with at least 2-fold differences between *mdx* hearts injected with vehicle (Mdx+Vehicle) or CDCs (Mdx+CDC) (A). Each column represents an *mdx* heart and each row a gene. Probe set signal values were normalized to the mean across *mdx* hearts. The relative level of gene expression is depicted from the lowest (green) to the highest (red), according to the scale shown on top. Examples of fold changes of transcripts for genes involved in the various pathways of interest are plotted in panels D-F. G: Western blots and pooled data for protein abundance of catalase, superoxide dismutase-2 (SOD-2), and catalytic subunit of glutamate-cysteine ligase (GCLC) in wild-type (WT) or *mdx* mouse hearts 3 weeks after administration of vehicle (Veh.) or CDCs (CDC). CS: Citrate synthase loading control. *Data are means ± SEM; #P<0.05 vs. Mdx+CDC; †P<0.05 vs. Mdx+Vehicle and WT (wild type).*

Figure S2. *Related to Figure 1; Diminished cardiac fibrosis and collagen content and differential expression of genes involved in inflammation 3 weeks after CDC injection in* mdx *hearts.*

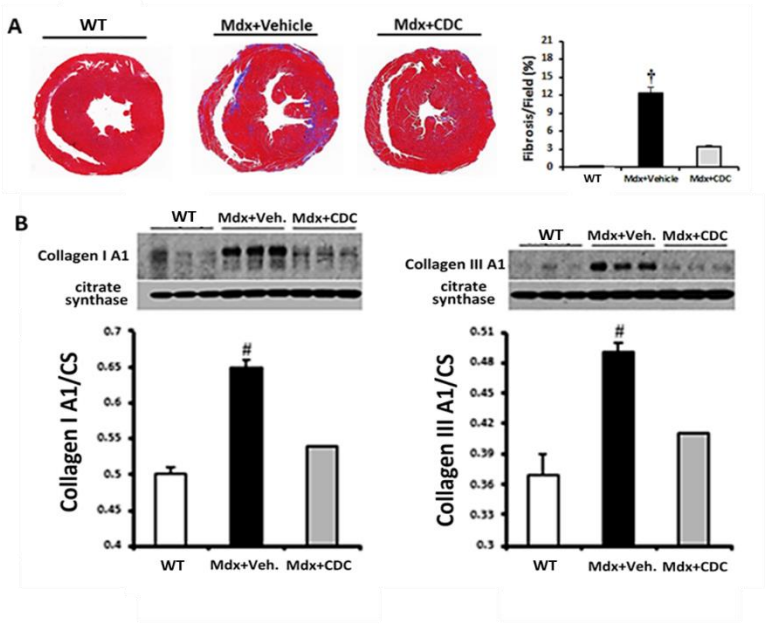

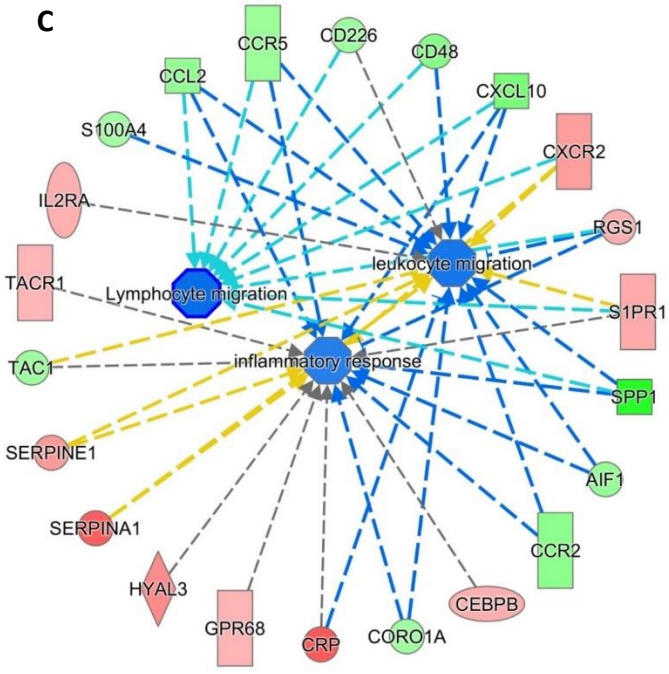

A, left panel: Representative Masson trichrome images of a wild-type heart (WT), an *mdx* heart that had been vehicle-injected (Mdx+Vehicle) and an *mdx* heart that had been CDC-injected (Mdx+CDC). A, right panel: pooled data for morphometric analysis. B: western blots and pooled data for myocardial cardiac collagen IA1 and IIIA1. C: Ingenuity pathway analysis of differentially expressed genes involved in inflammation in CDC/Vehicle *mdx* hearts, denoting inhibition of inflammatory response concomitantly with reduced migration of inflammatory cells in *mdx* hearts 3 weeks after CDC treatment. The blue color represents inhibition of function/response and the red and green colors represent up and downregulation, respectively. Data are means ± SEM; †$P<0.05$ vs. Mdx+CDC and WT (wild type); #$P<0.05$ vs. Mdx+CDC and WT (wild type); Scale Bar: 1mm.

Figure S3. *Related to Figure 1; Numbers of mitochondria from TEM images, mitochondrial DNA copy numbers (per nuclear genome) and cardiomyogenesis in* mdx *heart tissue 3 weeks after injection with vehicle (Veh.) or CDCs.*

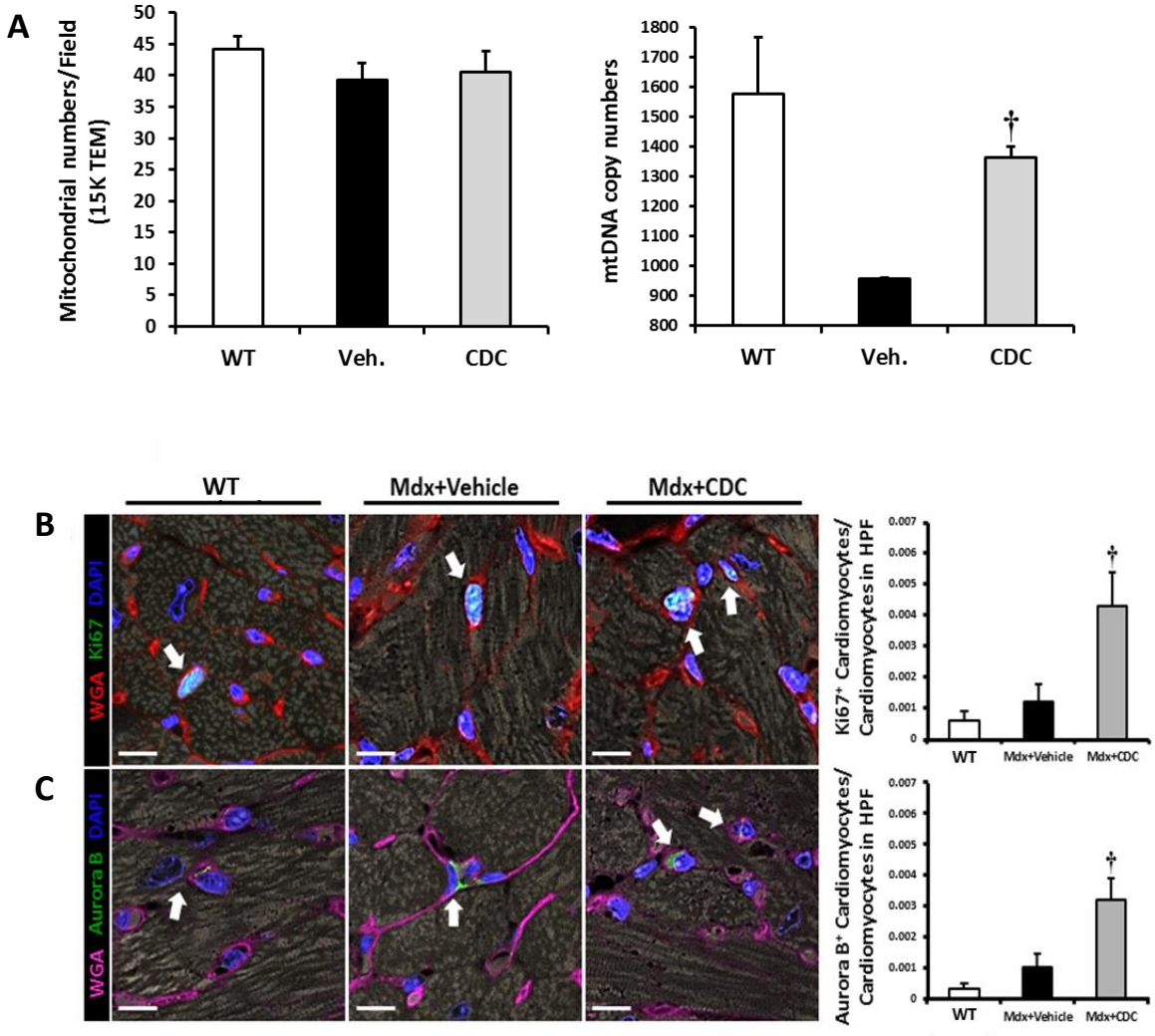

Numbers of mitochondria from TEM images (A; left panel) and mitochondrial DNA copy numbers (per nuclear genome) in *mdx* heart tissue (A; right panel) 3 weeks after injection with vehicle (Veh.) or CDCs. WT: age-matched wild-type mouse hearts. Enhanced cardiomyogenesis 3 weeks after CDC injection in *mdx* mice is evident from representative immunohistochemical images and pooled data (WT [wild type], vehicle- [Mdx+Vehicle] and CDC-treated [Mdx+CDC] *mdx* mouse hearts stained for Ki67 [B] and Aurora B [C]; n=4-6 per group). Arrows point to $Ki67^+$ (B) and aurora B^+ (C) cardiomyocytes. HPF: high power field. Data are means ± SEM; †$P<0.05$ vs. Mdx+Vehicle and WT (wild type); Scale bars: 10µm.

Fig. S4. *Related to Figure 2; Properties of exosomes isolated by ultracentrifugation from hypoxic CDCs: size distributions, physiological responses and immunogenicity.*

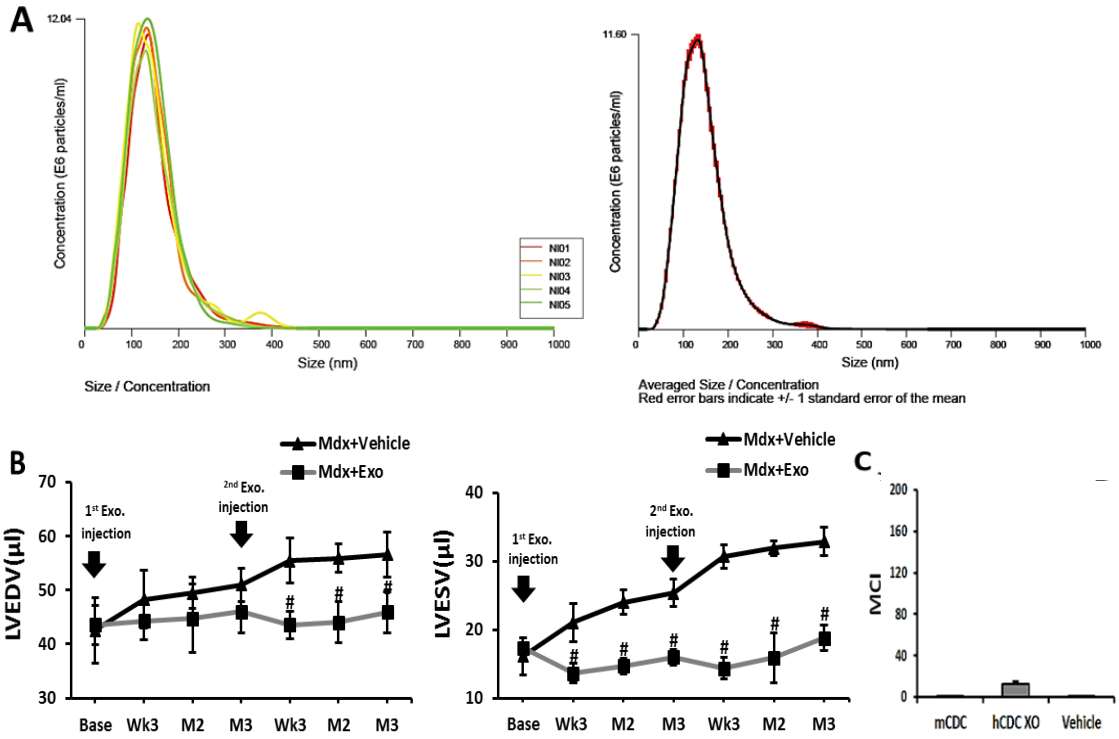

A: Exosomes isolated by ultracentrifugation were analyzed by nanoparticle tracking, using the NanoSight NS300 system (NanoSight Ltd, UK). Videos were collected and analyzed using NTA-software (version 2.3), with the minimal expected particle size, minimum track length, and blur setting all set to automatic. Camera shutter speed was fixed at 30.01 ms and camera gain was set to 500. Camera sensitivity and detection threshold were set close to maximum (15 or 16) and minimum (3 or 4), respectively, to reveal small particles. Ambient temperature was recorded manually, ranging from 24 to 27°C. For each sample, five videos of 60 seconds duration were recorded, with a 10-second delay between recordings, generating five replicate histograms that were averaged. Representative five replicate histograms depicting size/concentration (A; left graph). Standard error of the mean concentration, calculated from 5 replicates, is shown in red in right graph. B: LV end-diastolic (LV EDV) and end-systolic (LV ESV) volumes after CDC exosome (Exo) administration. CDC-exosome transplantation resulted in a sustained improvement of LV ESV for 3 months after both first and second (3 months later) injections in *mdx* muse hearts relative to placebo. Differences in LV EDV were significant only after the second injection. C: IgG serum levels 6 months after the first injection and 3 months after repeat injection of mouse CDCs (mCDC), human CDC exosomes (hCDC XO) and vehicle in *mdx* mice. Circulating anti-donor IgG antibodies were screened by flow cytometry. Pooled data are means ± SEM. # *P<0.001* vs Mdx+Exo.

Figure. S5. *Related to Figure 3; Secondary effects of intramyocardial CDC injection on remote tissues.*

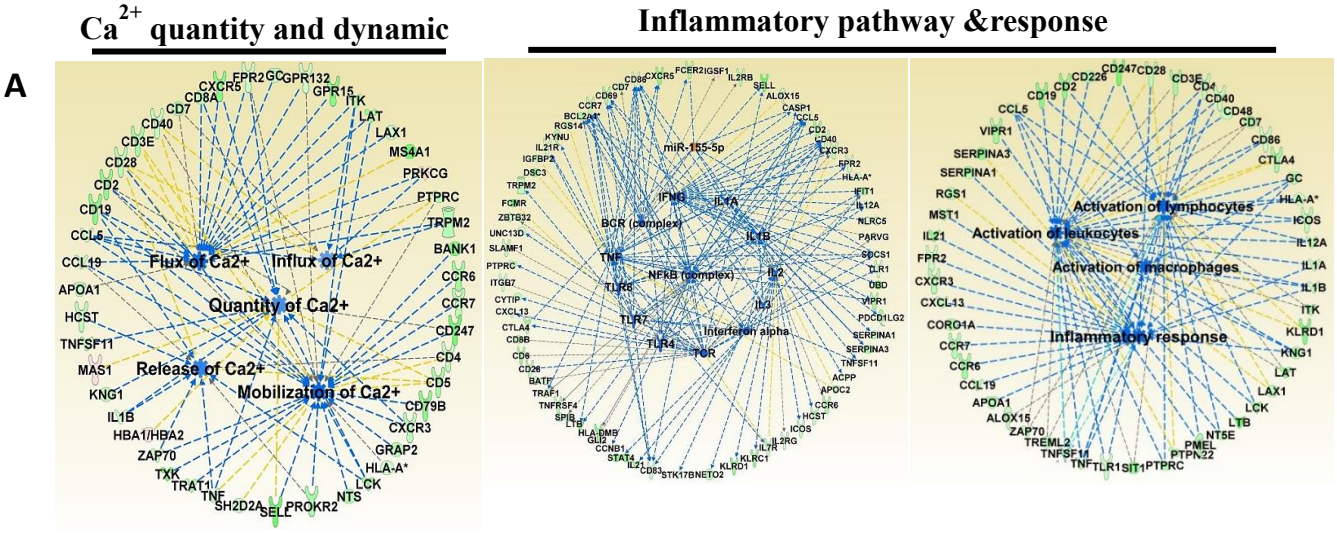

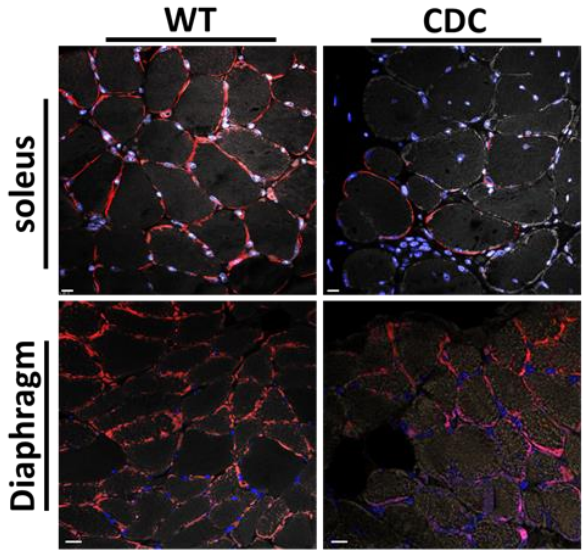

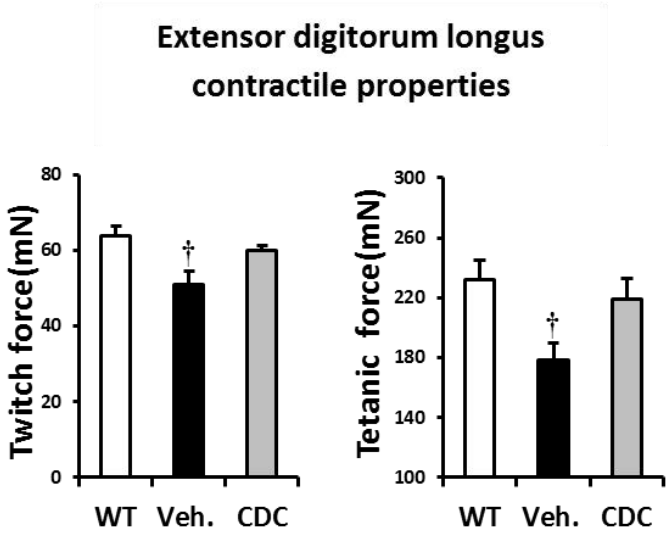

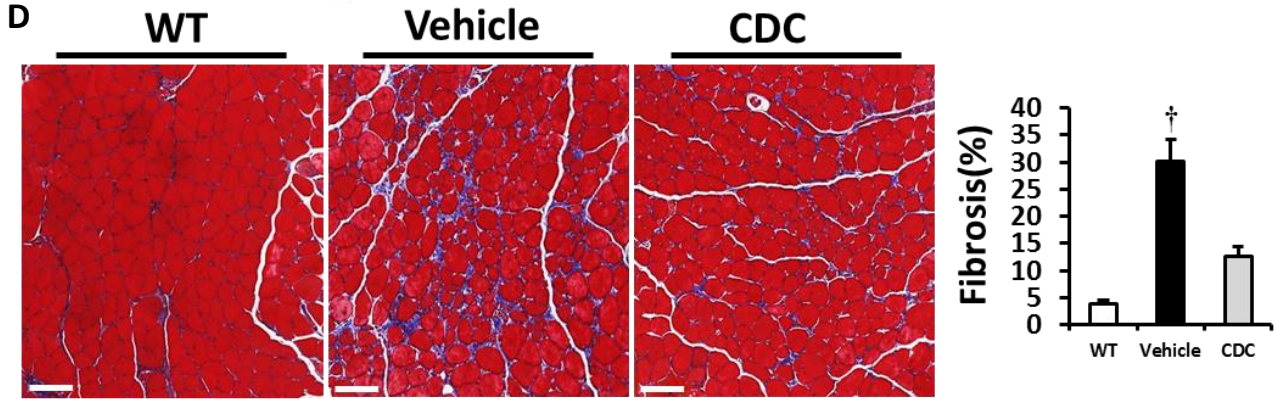

A: Ingenuity pathway analysis of differentially expressed genes involved in Ca^{2+} dynamics and inflammation in diaphragm of *mdx* mice treated intramyocardially with CDC or vehicle, denoting improved Ca^{2+} dynamic and inhibition of NF-κB inflammatory pathway and inflammation in *mdx* diaphragm. Blue color represents inhibition of function/response and the red and green colors represent up and downregulation, respectively. B: Dystrophin expression in soleus and diaphragm muscles of *mdx* mice 3 weeks after treatment. Representative immunohistochemical images of soleus and diaphragm from wild type control (WT) and *mdx* mice intramyocardially-injected with CDCs (CDC) stained for dystrophin. C: Extensor digitorum longus (EDL) contractile properties after intramyocardial CDC injection: *In vitro* measurement of EDL isometric twitch force and maximum tetanic force in controls (WT) and 3 weeks after injection of vehicle (Veh.) or CDCs (CDC) into *mdx* hearts. D: Diminished fibrosis in *mdx* soleus muscles 3 weeks after intramyocardial CDC injection (CDC) relative to vehicle; WT: wild-type control. Representative Masson trichrome images (left) and pooled data for morphometric analysis. *Data are means ± SEM; †P<0.005 vs. CDC and WT (control); Scale bars: 10μm (B); 100 μm (D).*

Figure S6. *Related to Figure 3 and Figure 4; Non-cardiac manifestations of CDC or CDC exosome injections and fold changes of microRNAs in CDC exosomes isolated from hypoxic conditioned media compared to CDC exosomes isolated from normoxic conditioned media.*

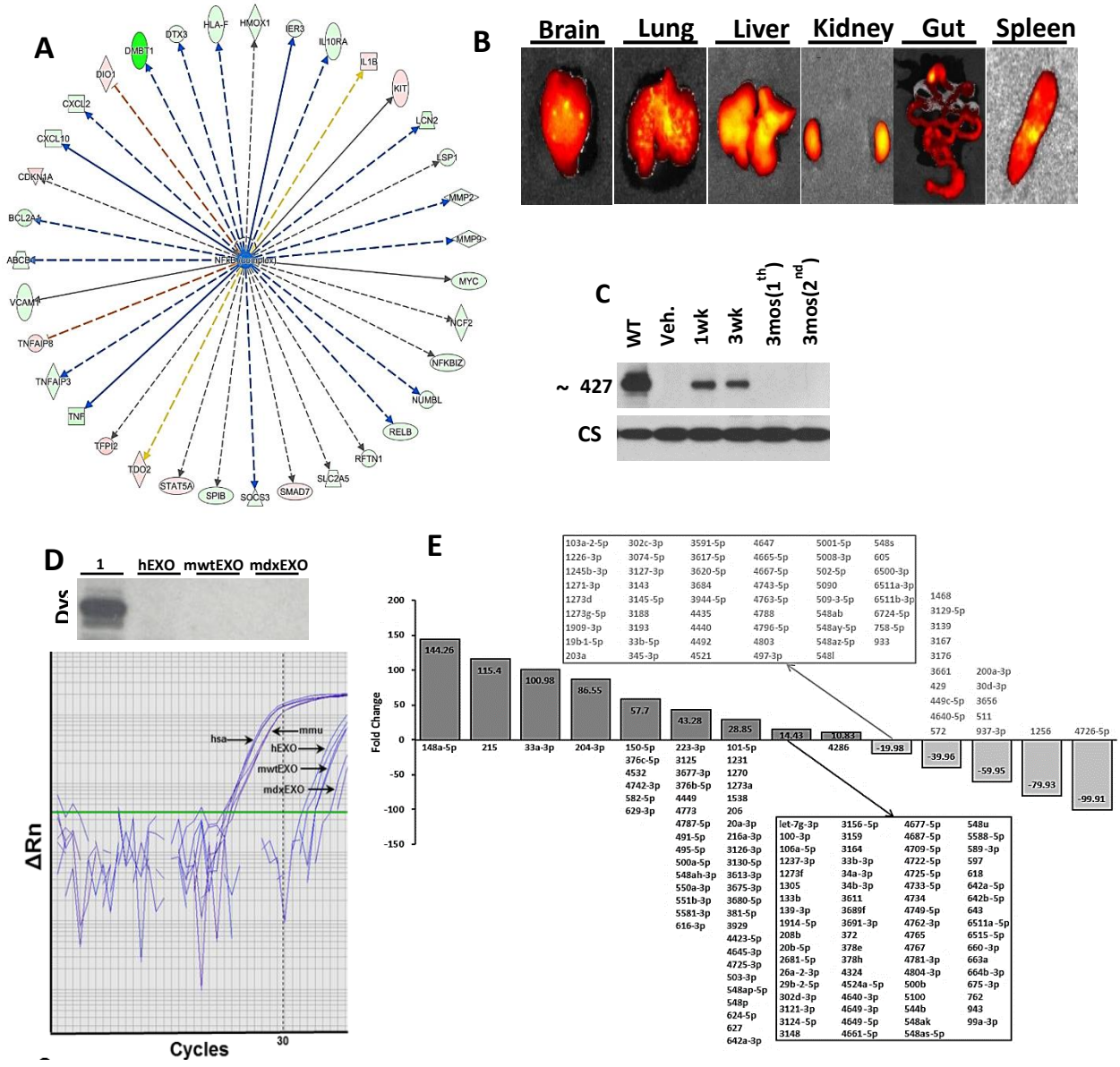

A: Ingenuity pathway analysis of differentially expressed genes involved in inflammation in liver of *mdx* mice injected intramyocardially with CDCs or vehicle, showing inhibition of NF-κB inflammatory pathway in *mdx* livers 3 weeks after intramyocardial CDC injection. The blue color represents inhibition of function/response and the red and green colors represent up and downregulation, respectively. B: Bioluminescence imaging of *mdx* mouse organs after systemic injection of dyed human CDC exosomes. Six hours after injection of exosomes systemically into the *mdx* mouse left ventricular cavity, the indicated organs were dissected and imaged using IVIS molecular imaging systems (Caliper Life Sciences, Hopkinton, MA, USA). C: Western blot of dystrophin protein in wild type control (WT) mouse heart and *mdx* mouse hearts 1 week, 3 weeks and 3 months after first intraventricular CDC-exosome injection and 3 months after second (repeat) CDC-exosome injection. D: Immunoblot probing for full length dystrophin protein in CDC-exosomes from human (hEXO), wild-type mouse (mwtEXO), and *mdx* mouse (mdxEXO). No detection of dystrophin protein in exosomes isolated from any CDC source. E: qPCR reaction for dystrophin on human (hsa) and mouse (mmu) heart tissues (positive controls) and on exosomes isolated from human CDCs (hEXO), mouse wild-type CDCs (mwtEXO), and *mdx* mouse CDCs (mdxEXO). All reactions for CDC-exosomes were flagged for empty well, demonstrated dystrophin mRNA below detection limits by quantitative PCR. F: Fold changes of microRNAs in CDC exosomes isolated from hypoxic conditioned media (2% O_2) compared to CDC exosomes isolated from normoxic conditioned media; fold change >10 and <-20 were included. NEBNext Small RNA Library Prep kit (New England BioLabs, Ipswich, MA) was used for miRNA-seq library preparation of extracted small RNAs from the exosomes. RNAs were extracted from exosomes using miRNeasy Serum/Plasma Kit (QIAGEN, Germantown, MD).

Figure S7. *Related to Figure 7; Sashimi plots of RNA-Seq data for dystrophin from WT (wild type) and vehicle-, CDC-, CDC-exosome- and miR-148a treated* mdx *hearts and verification that the bioactivity of the extracellular vesicles studied here is indeed attributable to exosomes characterized by the most rigorous of criteria.*

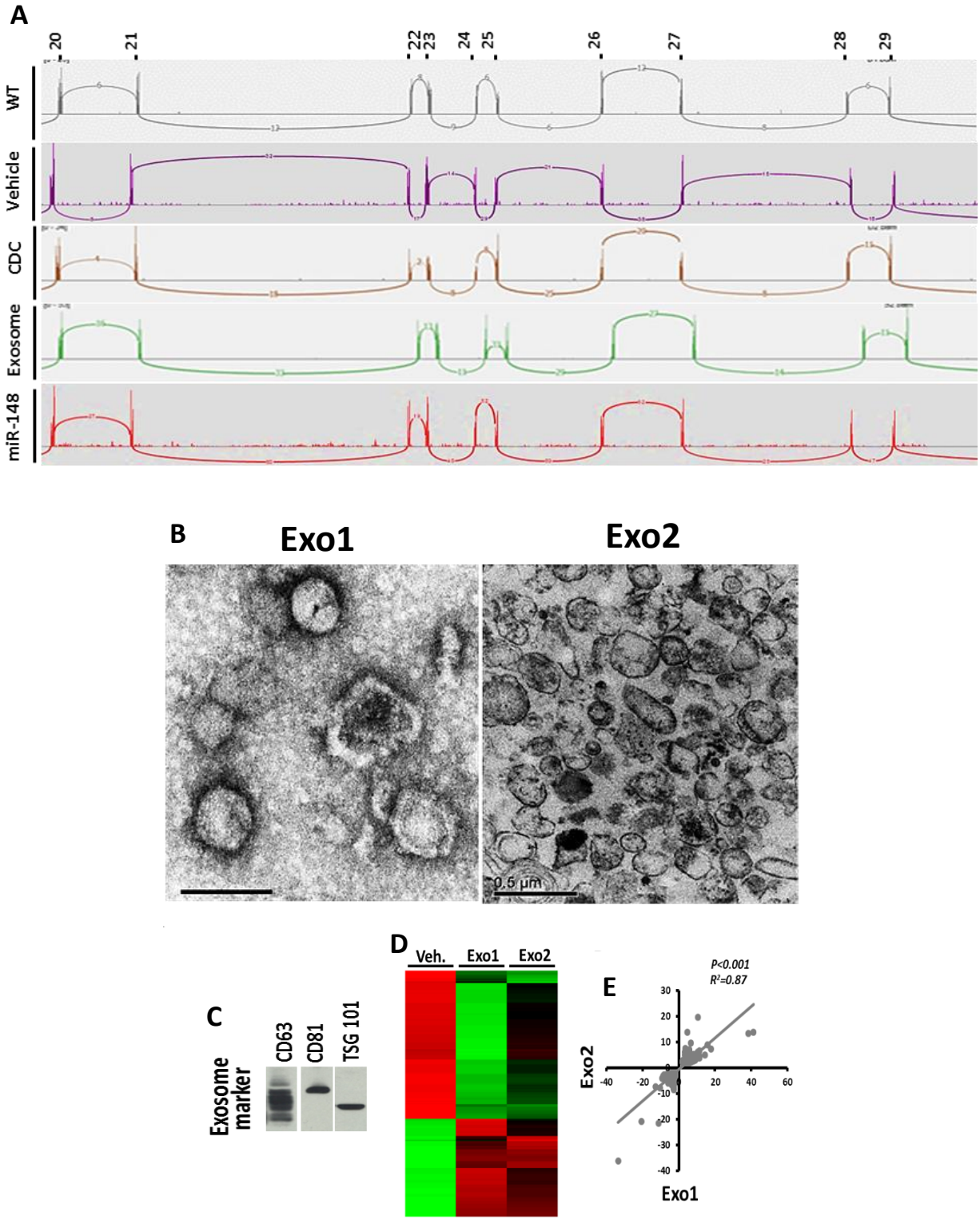

A: Sashimi plots of RNA-Seq data for dystrophin from WT (wild type) and vehicle-, CDC-, CDC-exosome- and miR-148a treated *mdx* hearts depict no junction read spanning exon 23. B-E: Verification that the bioactivity of the extracellular vesicles studied here are indeed attributable to exosomes characterized by the most rigorous of criteria (Lötvall et al., 2014). We floated the exosomes on a linear iodixanol density gradient, demonstrated vesicles by transmission electron microscopy (TEM) and the presence of key membrane proteins, and show that the biological effect truly is vesicle associated. B: TEM images of sequentially-centrifuged exosomes with (Exo1, left) and without (Exo2, right) purification with linear iodixanol density gradient show vesicles in both conditions. The vesicles are variable in size and morphology, consistent with previous work (Zabeo et al., 2016). C: Western blot on lysed exosomes for key proteins characteristic of exosomes: CD63, CD81 and TSG. D: Biological activity of Exo1 and Exo2 were compared by injection into *mdx* soleus muscles and evaluation of *mdx* soleus transcriptome 3 weeks after injection. Changes in *mdx* soleus transcriptome 3 wks after Exo1 and Exo2 injection. 2-Dimensional hierarchical clustering using 332 genes with at least 2-fold differences between vehicle/Exo1 and vehicle/Exo2 in *mdx* soleus muscles. E: Correlation of fold changes in expression of same genes 3 weeks after Exo1 and Exo2 injection in *mdx* soleus muscles. The similarity of the effects of Exo1 and Exo2 support the notion that the bioactivity of the vesicles isolated by our default protocol (cf. Fig. S9) is genuinely due to exosomes, and not to other types of vesicles that might have been co-purified by ultracentrifugation; Scale bars: 50μm (Exo1); 100 nm (Exo2).

Assessment of CDC engraftment and dystrophin mRNA in exosomes by real-time polymerase chain reaction

Quantitative polymerase chain reaction (PCR) was performed 1, 2 and 3 weeks after CDC injection to assess cell engraftment. Male CDCs were injected into female *mdx* mice to enable detection of the SRY gene located on the Y chromosome as a marker of engraftment using the TaqMan assay (Applied Biosystems, Foster City, CA)(Li et al., 2012). The whole mouse heart was harvested, weighed, and homogenized. A standard curve was generated with multiple dilutions of genomic DNA isolated from the same batch of CDCs injected. All samples were spiked with equal amounts of genomic DNA from non-injected mouse hearts as a control. For each reaction, 50 ng of genomic DNA was used. Real-time PCR was performed in triplicate. Engraftment was quantified from the standard curve. Percentage engraftment of CDCs at 1 week was ~8% and <1% at 2 weeks. By 3 weeks, no surviving CDCs could be detected. **Dystrophine mRNA in exosomes:** Standard Sybr green qPCR reactions were setup starting with 500 ng of cDNA from human (hsa) and mouse (mmu) heart tissues (positive controls) and from exosomes isolated from human CDCs (hEXOs), mouse wild-type CDCs (mwtEXO), and *mdx* mouse CDCs (mdxEXOs). Average Ct values were figas follows: hsa control (23.4), mmu control (24.0), hEXO (33.8), mwtEXO (35.0), mdxEXO (36.8). All reactions for CDC-exosomes were flagged for empty well. Primers for all qPCR reactions are listed in panel below.

Gene	Accession No.	Sequence (5' → 3')
DMD (mmu)	XM_006527767	F: TCAGTCCAGAAGCCCATGAAC R: GGACAAAACCCACTCGCTAGA
DMD (hsa)	NM_004006	F: GTCCCTCTCTGCGTGGATATG R: CCGCTTCGATCTCTGGCTTAT

Respirometry

Mice were sacrificed via cervical dislocation after isofluorane anesthesia. Hearts were immediately excised, rinsed in PBS and homogenized via polytron in 1mL ice cold HES buffer (250mM sucrose, 1mM EDTA, 10mM HEPES, pH 7.4). Lysates were spun down at 1000*g* for 5min at 4^{o}C to remove unbroken cells and large debris. Supernatant was then spun down at 7000*g* for 10min at 4^{o}C to separate mitochondria-enriched fraction from crude cytosol. The pellet was resuspended in 1mL HES buffer (A subportion in lysis buffer for WB). Protein quantification was performed and adjusted with HES buffer to obtain sample containing 10µg protein in 50µL buffer which was loaded into a 24-well Seahorse cell culture plate, which was spun down at 2000*g* for 20min at 4^{o}C to allow mitochondria to adhere to the plate surface. 450µL MAS buffer (70mM sucrose, 220mM mannitol, 5mM KH2PO4, 5mM MgCl2, 1mM EGTA, 0.2% fatty acid-free BSA, pH 7.4) was then added prior to Seahorse XF24 mitochondria stress test. 5mM/5mM pyruvate/malate and 0.25mM ADP were used to stimulate mitochondrial oxidative phosphorylation followed by 1µM oligomycin, 1µM FCCP, and a mixture of 1µM antimycin, 500nM rotenone. Citrate synthase activity was measured in sample lysates to normalize for the actual amount of mitochondria loaded for the test. Seahorse respirometry on normal and Duchenne iPS cell-derived cardiomyocytes was performed using Seahorse™ XF96 Extracellular Flux analyzer as described (Guan et al., 2014).

Bioluminescence imaging of *mdx* mouse organs after systemic injection of fluorescently-labeled CDC-exosomes

Six hours after injection of fluorescently-labeled CDC-exosomes systemically into the *mdx* mouse left ventricular cavity, the mice were sacrificed and the organs dissected and imaged using an IVIS molecular imaging system (Caliper Life Sciences, Hopkinton, MA, USA).

Intracellular Ca^{2+} recordings

iPS- derived cardiomyocytes were loaded for 30 min with 5 μM of the fluorogenic calcium-sensitive dye, Cal-520 (AAT Bioquest, Sunnyvale, CA) and paced via field stimulation at a frequency of 1 Hz using an Ion-Optix Myopacer (IonOptix Corp) delivering 0.2 ms square voltage pulses with an amplitude of 20 V via two platinum wires placed on each side of the chamber base (~1 cm separation). We used the xyt mode (2D) of a Leica TCS-SP5-II (Leica Microsystems Inc.; Wetzlar, Germany) to image intracellular Ca^{2+}. Cal- 520 was excited with a 488 nm laser and its emission (>505 nm) was collected with a 10X objective (Leica: N PLAN 10x/0.25) at scan speeds ranging from 36 to 7 ms per frame depending on the field size. The fluorescence intensity (F) proportional to Ca^{2+} concentration was normalized to baseline fluorescence, F0 (F/F0). Time to peak and Ca^{2+} transient amplitude (F/F0) were analyzed with the software Clampfit (ver. 10.2, Molecular Devices, Inc.). Beat-to-beat alternans in each group was calculated over 5-10 sec intervals of pacing at 1 Hz. The amplitude of each transient from each cell (n=10 cells in each group) was measured during pacing and mean and standard deviation were compared among groups.

RNA sequencing and 2-Dimensional hierarchical clustering

Nugen Ovation RNA-Seq System V2 kit was used to generate double-stranded cDNA using a mixture of random and poly (T) priming. Kapa LTP library kit (Kapa Biosystems, Wilmington MA) was used to make the sequencing library. The workflow consists of fragmentation of double stranded cDNA, end repair to generate blunt ends, A-tailing, adaptor ligation and PCR amplification. Different adaptors were used for multiplexing samples in one lane. Sequencing was performed on Illumina HiSeq 2500 for a pair read 100 run. Data quality check was done on

Illumina SAV. Demultiplexing was performed with Illumina CASAVA 1.8.2. The reads were first mapped to the latest UCSC transcript set using Bowtie2 version 2.1.0 and the gene expression level was estimated using RSEM v1.2.15 (Accession number: GSE85888). TMM (trimmed mean of M-values) was used to normalize the gene expression. Differentially expressed genes were identified using the edgeR program. Genes showing altered expression with $p<0.05$ and more than 2 fold changes were considered differentially expressed. The pathway and network analyses were performed using Ingenuity pathway analysis (IPA). IPA computes a score for each network according to the fit of the set of supplied focus genes. These scores indicate the likelihood of focus genes to belong to a network versus those obtained by chance. A score > 2 indicates ~99% confidence that a focus gene network was not generated by chance alone. The canonical pathways generated by IPA are the most significant for the uploaded data set. Fischer's exact test with FDR option was used to calculate the significance of the canonical pathway. 2-Dimensional hierarchical clustering used genes with at least 2 times fold change difference (log_2) between vehicle/CDC, mutant/CDC-exosome (intraventricular injection) or CDC (intramyocardial)/ CDC-exosome (intraventricular injection) *mdx* hearts, diaphragms, soleus and EDL muscles. Each column represents an *mdx* analyzed tissue and each row a gene. Probe set signal values were normalized to the mean across *mdx* analyzed tissues. The relative level of gene expression is depicted from the lowest (green) to the highest (red), according to the scale shown; examples of fold changes of transcripts for genes involved in the various pathways of interest are plotted.

Cardiac mitochondria after intramyocardial CDC injection

TEM images of sections from apical, middle and basal parts of each heart were used for calculating the average numbers of mitochondria in WT (wild type) and CDC/vehicle *mdx* mouse hearts. Extracted DNAs (QIAamp DNA Mini Kit, QIAGEN, Germantown, MD) from whole heart tissue

were used to measure mitochondrial to nuclear DNA ratio using PCR format per manufacturer's instructions (NovaQUANT™ Mouse Mitochondrial to Nuclear Ratio kit, EMD Millipore, Billerica, MA).

Authentication

The CDC cell lines were authenticated by karyotype, antigenic, phenotype, and PCR viral and mycoplasma assessments. The pluripotency of the iPSCs was confirmed by 1) PCR array of pluripotency associated genes; 2) immunostaining for critical pluripotent markers such as OCT-4, SOX-2, SSEA4 and Tra-1-60, Tra-1-81. 3) teratoma assay by engrafting iPS in the kidney capsule of SCID mice.

Echocardiography

Echocardiographic studies were performed two days before (Baseline) and 3 weeks, 2 and 3 months after first CDC/CDC-exosome (CDC-exosome) or vehicle injection and 3 weeks, 2 and 3 months after second CDC/CDC-exosome or vehicle injection (when applicable) using the Vevo 770 Imaging System (VisualSonics, Toronto, Canada)(Smith et al., 2007). The same imaging system was used to perform echocardiographic studies at baseline (2 days before) and 3 weeks after selected RNA (or control) injection. After induction of light general anesthesia, the heart was imaged at the level of the greatest LV diameter. LV ejection fraction (LVEF) was measured with VisualSonics version 1.3.8 software from 2-dimensional long-axis views.

Treadmill exercise testing and survival analysis

For Fig. 1B, exercise capacity was assessed weekly with Exer-3/6 open treadmill (Columbus Instruments, Columbus, OH), beginning 1 week pre-operatively and 3 weeks after CDC/vehicle

injection (exercise capacity measured in a subset of *mdx* mice 1 week pre-operatively was equivalent to that measured 3 weeks post-operatively in the Mdx+Vehicle group). After an acclimation period (10 m/min for 20 min), stepwise increases in average speed (2 m/min) were applied every two minutes during treadmill exercise until the mouse became exhausted (spending >10 seconds on shocker; continuous nudging was used during treadmill to help mice stay on the track). Subsequently, the mouse was returned to the cage and the total distance recorded. The treadmill protocol conformed to guidelines from the American Physiological Society(Kregel et al., 2006). After 3 months of weekly exercise, CDC/vehicle *mdx* mice along with wild-type age-matched mice were followed for assessment of mortality (Fig. 1C).

In vitro isometric contractile properties of skeletal muscle

Mice were deeply anesthetized with Ketamine/Xylazine (80 mg/kg and 10 mg/kg body weight IP), the soleus (SOL) and/or extensor digitorum longus (EDL) and/or diaphragm (DIA) muscles were rapidly excised, and the animal was euthanized. Briefly, following a lateral midline skin incision of the lower leg the SOL and/or EDL muscle was dissected and isolated and its tendons of origin and insertion were tightened with silk suture (3-0) and rapidly excised. The SOL or EDL muscle was vertically mounted in a tissue bath containing a mammalian Ringer's solution of the following composition: (in mM) 137 NaCl, 5 KCl, 2 $CaCl_2$, 1 $MgSO_4$, 1 NaH_2PO_4, 24 $NaHCO_3$, 11 glucose. The solution was constantly aerated with 95% O_2 and 5% CO_2 with pH maintained at 7.35 and temperature kept at 24°C. For studies of the diaphragm, following a left costal margin skin and muscle incision, a section of the midcostal hemidiaphragm was transferred to a preparatory Sylgar-lined dish containing cold Ringer’s and a narrow 3-4 mm wide strip of diaphragm was isolated maintaining fiber attachments to the rib and central tendon intact which were tighten with silk suture and mounted vertically in the tissue bath. One end of the SOL, EDL or DIA was secured to

a clamp at the bottom of the dish and one end was attached to a calibrated force transducer (Cambridge Technology Model 300B, Watertown, MA). A micromanipulator linked to the system was used to adjust muscle length. Platinum plate electrodes placed on each side of the muscle were used for direct muscle stimulation (Grass Model S88 stimulator; Quincy, MA) using 0.2 msec duration monophasic rectangular pulses of constant current delivered at supramaximal intensity. Muscle length was adjusted until maximum isometric twitch force responses were obtained. Isometric contractile properties were determined at optimal length (Lo). Peak twitch force (Pt) was determined from a series of single pulses. Force/frequency relationships were measured at stimulus frequencies ranging from 5-150 pulses per second (pps). The stimuli were presented in trains of 1 sec duration with an interval of at least 1 min intervening between each stimulus train. Muscle forces generated, including Pt and maximum tetanic force (Po), were normalized for the estimated physiological cross-sectional areas (CSA) of the muscle segment (CSA = muscle weight/1.056 x Lo; where 1.056 g/cm^3 represents the density of muscle) and expressed in Newtons (N)/cm^2. For the SOL and EDL muscle Lo was also normalized for muscle fiber length (0.71 and 0.44 of Lo, respectively) in estimating muscle specific force. Absolute muscle forces generated by the SOL and EDL are also reported (mN)(Fournier and Lewis, 2000).

Histology

Mice were sacrificed 3 weeks (WT: n=4; Mdx+Vehicle: n=6; Mdx+CDC/Mdx+CDC-exosome: n=6 each) or 3 months (WT: n=4; Mdx+Vehicle: n=6; Mdx+CDC/Mdx+CDC-exosome: n=6) after first CDC/CDC-exosome injections (n=6). Paraffin-embedded sections from apical, middle and basal parts of each heart or from diaphragm or entire soleus muscle (cross or longitudinal sections) were used for histology. Masson's trichrome staining (HT15 Trichrome Stain [Masson] Kit; Sigma-Aldrich, St. Louis, MO) was performed for evaluation of fibrosis. T cells, B cells and

macrophages were assessed by immunostaining with antibodies against mouse CD3, CD20 and CD68, respectively, and the average number of cells was calculated by counting cells in 10 fields from each of 10 sections selected randomly from the apical (3 sections; 50µm interval), middle (4 sections; 50µm interval) and basal (3 sections; 50µm interval) regions of each heart or from diaphragm. The data were presented as number of cells/mm^2 field. Actively-cycling ($Ki67^+$) and proliferating (Aurora B^+) cardiomyocytes were counted in the same manner, and the cycling and proliferating fractions were expressed as the number of $Ki67^+$, Aurora B^+ divided by the total number of cardiomyocytes per high-power field (HPF), respectively, as described(Aminzadeh et al., 2015). Measurements were averaged for each heart. Immunofluorescence staining: Heat-induced epitope retrieval in low or high pH buffer (DAKO, Carpinteria, CA) was followed by 2 hours permeabilization/blocking with Protein Block Solution (DAKO, Carpinteria, CA) containing 1% saponin (Sigma, St. Louis, MO; Protein Block Solution contained 3% saponin was applied for immunofluorescence staining of Ki67). Subsequently, primary antibodies in Protein Block Solution were applied overnight in 4 C° for immunofluorescence staining of 5-µm sections from apical, middle and basal parts of each heart or cross sections of soleus muscle. After 3x wash with PBS, each 10 minutes, Alexa Fluor secondary antibodies (Life Technologies, Grand Island, NY) were used for detection. Images were taken by a Leica TCS SP5 X confocal microscopy system. Immunofluorescence staining was conducted using antibodies against Ki-67 (SP6; RM-9106-S0; 1:50, Thermo Fisher Scientific, Fremont, CA), WGA (Wheat germ agglutinin; W32466, 1:200; Thermo Fisher Scientific, Fremont, CA), Nrf2 (C20; 1:50; Santa Cruz Biotechnology, Santa Cruz, CA), aurora B (611082; 1:250; BD Biosciences, San Jose, CA). Immunoperoxidase staining: Immunohistochemical detection of CD3 (AC-0004A), CD20 (AC-0012A) and CD68 (790-2931) was performed on 5-µm sections using prediluted rabbit monoclonal antibodies from Ventana

Medical System (Tuscon, AZ; CD68) and Cell Marque (Rocklin, CA; CD3, CD20). Staining was conducted on the Leica Bond-Max Ventana automated slide stainer (Chicago, IL) using onboard heat-induced epitope retrieval method in high pH ER2 buffer (Leica Biosystems, Buffalo Grove, IL). Staining was visualized using the Dako Envision^{+} rabbit detection System and Dako DAB (Carpinteria, CA). The slides were subsequently counterstained with mayer's hematoxylin for 1 minute and coverslipped. Electron microscopy: Apical (1 cube), middle (3 cubes from right, middle and left subparts) and basal (3 cubes from right, middle and left subparts) parts of posterior wall from each heart (WT: n=3; Mdx+Vehicle: n=3; Mdx+CDC: n=3) were fixed by immersion of 1mm^3 cubes in 2% glutaraldehyde, postfixed in osmium, and embedded in epon. Sections were cut at silver thickness, stained with uranyl acetate and lead citrate, and viewed with JEOL 1010 equipped with AMT digital camera system.

Western blots

Western blot analysis was performed to compare abundance of target proteins contributing to Nrf2 signaling [Nrf2, phospho-Nrf2 (Nrf2-p^{s40}) and Nrf2 downstream gene products: heme oxygenase-1 (HO-1), catalase, superoxide dismutase-2 (SOD-2), and catalytic subunit of glutamate-cysteine ligase (GCLC)], Nrf2 phosphorylation [phospho-Akt(Akt-p^{308}; Akt-p^{473})], oxidative phosphorylation [CI (NDUFB8 subunit), CII (SDHB subunit), CIV (MTCO1 subunit), CIII (UQCRC2 subunit) and CV (ATPSA subunit)], inflammation (NF-κB and MCP-1), fibrosis (Collagen IA1 and collagen IIIA1) and myofiber proliferation and differentiation (Myogenin, MyoD and IGF1R). Density of malondialdehyde protein adducts, a marker of oxidative stress, was also measured by Western blotting (WB). Samples from apical, middle and basal parts of each heart (each 1 mm-thick transverse section) were mixed and homogenized, and nuclear and cytoplasmic fractions were extracted per manufacturer's instructions (CelLytic NuCLEAR

Extraction Kit, Sigma-Aldrich, St. Louis, MO). The same kit was applied for extraction of nuclear and cytoplasmic fractions from entire soleus muscle, a narrow 3-4 mm wide strip of the left midcostal hemidiaphragm and iPSC derived cardiomyocytes. Mitochondria were extracted from fresh whole hearts (WT: n=3; Mdx+Vehicle: n=8; Mdx+CDC: n=8) as described in respirometry section. Cytoplasmic, nuclear and mitochondrial extracts for WB analysis were stored at −80C°. The protein concentrations in extracts were determined by the Micro BCA Protein Assay Kit (Life technologies, Grand Island, NY). Target proteins in the cytoplasmic, nuclear and mitochondrial fractions were measured by Western blot analysis using the following antibodies: antibodies against mouse Nrf2 (C-20; sc-722) , HO-1 (H-105; sc-10789), catalase (H-300; sc-50508), SOD-2 (FL-222; sc-30080), GCLC (H-338; sc-22755), collagen IA1 (D-13; sc-25974), and collagen IIIA1 (S-17; sc-8780-R) were purchased from Santa Cruz Biotechnology (Santa Cruz, CA), phospho-Nrf2 (Nrf2-p^{s40}; orb34864; Biorbyt, San Francisco, CA), respiratory chain subunits (Total OXPHOS Rodent WB Antibody Cocktail antibody; MS604), malondialdehyde (ab27642), citrate synthase (ab96600) and TBP (TATA binding protein; ab63766) [Abcam, Cambridge, MA], Akt (9272) and Akt-p^{T308} (5106S) , IκB-α (4814S), p-IκB-α (9246S), phospho-NF-κB p65 (Ser536; 3033S) [Cell Signaling Technology, Denver, CO], MCP-1 (HPA019163), NF-κB p65 (SAB4502615) [Sigma-Aldrich, St. Louis, MO], Myogenin (F12B; MA5-11658), MyoD (5.8A; MA1-41017), Akt-p^{S47} (14-6; OMA1-03061) and IGF-IR/IGF1 Receptor (194Q13; AHO1292) [Thermo Fischer Scientific, Fremont, CA] antibodies were purchased from the cited sources. Antibodies to TBP and citrate synthase were used for measurements of the housekeeping proteins for nuclear (TBP), cytosolic and mitochondrial (citrate synthase) target proteins. Western blot methods: Briefly, aliquots containing 20 μg proteins were fractionated on 8, 10 and 4-12% Bis-Tris gel (Life technologies, Grand Island, NY) at 120 V for 2 h and transferred to a PVDF

membrane (Life technologies, Grand Island, NY). The membrane was incubated for 1 h in blocking buffer (1× TBS, 0.05% Tween-20 and 5% nonfat milk) and then overnight in the same buffer containing the given antibodies at optimal dilutions. The membrane was washed 3 times for 5 min in 1× TBS, 0.05% Tween-20 before a 2-h incubation in a buffer (1× TBS, 0.05% Tween-20 and 3% nonfat milk) containing horseradish peroxidase-linked anti-rabbit IgG (7074P2), anti-mouse IgG (7076S) [Cell Signaling Technology, Denver, CO] and anti-goat IgG (A5420; Sigma-Aldrich, St. Louis, MO) at 1:1000-3000 dilution. The membrane was washed 3 times for 5 min in 1 × TBS, 0.05% Tween-20 and developed by autoluminography using the ECL chemiluminescent agents (Super Signal West Pico Chemiluminescent Substrate; Life Technologies, Grand Island, NY). Citrate synthase and TBP were used as housekeeping proteins against which expressions of the proteins of interest were normalized. Phosphorylated Akt, Nrf2 and IκB-α were normalized to total Akt, Nrf2 and IκB-α. Western blot analyses of collagen I and collagen III were conducted under non-reducing, non-denaturing conditions.

Statistical analysis

All pooled data are presented as mean±SEM, except results for alternans data (Fig. 6A) which are presented as mean ±SD. Normality and equality of variances of data sets were first tested using Kolmogorov-Smirnov and Levene's tests, respectively. If both were confirmed, t-test or analysis of variance followed by Bonferroni's post hoc test were used for determination of statistical significance; if either normality or equality of variances was not assured, nonparametric tests (Wilcoxon test or Kruskal-Wallis test followed by Dunn's post-test) were applied (SPSS II, SPSS Inc., Chicago, Illinois). No preliminary data were available for a power analysis. Results from a pilot project allowed us to power subsequent studies. The study followed preclinical reporting standards, as described (Landis et al., 2012). Age-matched mice were randomly allocated to

experimental groups using computer generated randomization schedules (https://www.randomizer.org). Conduct of experiments and analysis of results and outcomes were performed in a blinded manner (allocation concealment and blinded assessment of outcome). There was no post-hoc exclusion of mice or data after the analysis before unblinding.

Ejection Fraction Data

Preliminary data were collected from a pilot study of 5 animals per group measuring ejection fraction at baseline, and again 3 weeks after treatment with cells or vehicle control in *mdx* and corresponding wild-type mice (C57BL/10ScSnJ). The measured treatment effect was approximately 4 units, with a time effect of approximately 1 unit, with group standard deviations of 3.5 units. We anticipated larger differences between groups over later time points with possible increase in measured variance. Therefore, with 12 animals per treatment group in the each of the *mdx* groups, and 7 wild-type control animals, the study had at least 80% power to detect a difference of 4.5 units or greater in treatment effect and 1.4 units or greater in time effect in a study design with 6 measurements per animal over time assuming a compound symmetry covariance structure, a correlation of 0.7 between measurements within animals over time, and a two-sided alpha of 0.05. (Power computed via PASS v. 11.0.).

Treadmill Data

Preliminary data were collected from a pilot study of 5 animals per group measuring treadmill distance (i.e., the distance ambulated before exhaustion, as described below) at baseline, and again 3 weeks after treatment with cells or vehicle control in *mdx* animals and corresponding wild-type animals. The measured treatment effect was approximately 150 meters, with limited differences observed over time in untreated groups. Group standard deviations were approximately 75 meters,

with more variation observed after treatment. We anticipated larger differences between groups over later time points with possible increase in measured variance. Therefore, with 11 animals per treatment group in the each of the transgenic groups, and 7 wild-type control animals, the study had at least 80% power to detect a difference of 100 meters or greater in treatment effect and changes of at least 30 meters over time in a study design with 12 measurements per animal over time assuming a compound symmetry covariance structure, a correlation of 0.7 between measurements within animals over time, and a two-sided alpha of 0.05. (Power computed via PASS v. 11.0.).

REFERENCES

Aminzadeh, M.A., Tseliou, E., Sun, B., Cheng, K., Malliaras, K., Makkar, R.R., and Marbán, E. (2015). Therapeutic efficacy of cardiosphere-derived cells in a transgenic mouse model of non-ischaemic dilated cardiomyopathy. European heart journal *36*, 751-762.

Fournier, M., and Lewis, M.I. (2000). Functional, cellular, and biochemical adaptations to elastase-induced emphysema in hamster medial scalene. Journal of Applied Physiology *88*, 1327-1337.

Guan, X., Mack, D.L., Moreno, C.M., Strande, J.L., Mathieu, J., Shi, Y., Markert, C.D., Wang, Z., Liu, G., and Lawlor, M.W. (2014). Dystrophin-deficient cardiomyocytes derived from human urine: new biologic reagents for drug discovery. Stem cell research *12*, 467-480.

Kregel, K.C., Allen, D.L., Booth, F.W., Fleshner, M.R., Henriksen, E.J., Musch, T., O'Leary, D., Parks, C., Poole, D., and Ra'anan, A. (2006). Resource book for the design of animal exercise protocols. American Physiological Society Bethesda, 1-80.

Landis, S.C., Amara, S.G., Asadullah, K., Austin, C.P., Blumenstein, R., Bradley, E.W., Crystal, R.G., Darnell, R.B., Ferrante, R.J., and Fillit, H. (2012). A call for transparent reporting to optimize the predictive value of preclinical research. Nature *490*, 187-191.

Li, T.-S., Cheng, K., Malliaras, K., Smith, R.R., Zhang, Y., Sun, B., Matsushita, N., Blusztajn, A., Terrovitis, J., and Kusuoka, H. (2012). Direct comparison of different stem cell types and subpopulations reveals superior paracrine potency and myocardial repair efficacy with cardiosphere-derived cells. Journal of the American College of Cardiology *59*, 942-953.

Lötvall, J., Hill, A.F., Hochberg, F., Buzás, E.I., Di Vizio, D., Gardiner, C., Gho, Y.S., Kurochkin, I.V., Mathivanan, S., Quesenberry, P.*, et al.* (2014). Minimal experimental requirements for definition of extracellular vesicles and their functions: a position statement from the International Society for Extracellular Vesicles. 2014.

Smith, R.R., Barile, L., Cho, H.C., Leppo, M.K., Hare, J.M., Messina, E., Giacomello, A., Abraham, M.R., and Marbán, E. (2007). Regenerative potential of cardiosphere-derived cells expanded from percutaneous endomyocardial biopsy specimens. Circulation *115*, 896-908.

Zabeo, D., Cvjetkovic, A., Lasser, C., Schorb, M., Lotvall, J., and Hoog, J.L. (2016). Exosomes purified from a single cell type have diverse morphology and composition. bioRxiv.